

Structural and kinetic analysis of *Schistosoma mansoni* Adenylosuccinate Lyase (*SmADSL*)

Larissa Romanello¹, Vitor Hugo Balasco Serrão¹, Juliana Roberta Torini de Souza¹, Louise E. Bird^{2,3}, Joanne E. Nettleship^{2,3}, Heather Rada^{2,3}, Yamini Reddivari^{2,3}, Ray J. Owens^{2,3}, Ricardo de Marco¹, José Brandão-Neto⁴, Humberto D'Muniz Pereira¹.

1- Laboratório de Biologia Estrutural, Instituto de Física de São Carlos, Universidade de São Paulo, 13563-120, São Carlos, SP, Brazil. 2- OPPF-UK, Research Complex at Harwell, Rutherford Appleton Laboratory, Oxford, OX11 0FA, UK. 3-Division of Structural Biology, University of Oxford, Wellcome Trust Centre for Human Genetics, Roosevelt Drive, Headington, Oxon, OX2 7BN, 4-Diamond Light Source, Harwell Science and Innovation Campus, Didcot, Oxfordshire, OX11 0DE, UK.

Corresponding Author. Humberto D'Muniz Pereira. E-mail hmuniz.pereira@gmail.com

Abstract

Schistosoma mansoni is the parasite responsible for schistosomiasis, a disease that affects about 218 million people worldwide. Currently, both direct treatment and disease control initiatives rely on chemotherapy using a single drug, praziquantel. Concerns over the possibility of resistance developing to praziquantel, have stimulated efforts to develop new drugs for the treatment of schistosomiasis. Schistosomes do not have the *de novo* purine biosynthetic pathway, and instead depend entirely on the purine salvage pathway to supply its need for purines. The purine salvage pathway has been reported as a potential target for developing new drugs against schistosomiasis. Adenylosuccinate lyase (*SmADSL*) is an enzyme in this pathway, which cleaves adenylosuccinate (ADS) into adenosine 5'-monophosphate (AMP) and fumarate. *SmADSL* kinetic characterization was performed by isothermal titration calorimetry (ITC) using both ADS and SAICAR as substrates. Structures of *SmADSL* in Apo form and in complex with AMP were elucidated by x-ray crystallography revealing a highly conserved tetrameric structure required for their function since the active sites is formed from residues of three different subunits. The active sites are also highly conserved between species and it is difficult to identify a potent species-specific inhibitor for the development of new therapeutic agents. In contrast, several mutagenesis studies have demonstrated the importance of dimeric interface residues in the stability of the quaternary structure of the enzyme. The lower conservation of these residues between *SmADSL* and human ADSL could be used to lead the development of anti-schistosomiasis drugs based on disruption of subunit interfaces. These structures and kinetics data add another layer of information to *Schistosoma mansoni* purine salvage pathway.

Highlights

- Crystal Structure of Adenylosuccinate Lyase Apo form and in complex with AMP from *Schistosoma mansoni*.
- Analysis of the dimer interface and structural stability as a potential chemotherapeutic target.
- Characterization of *SmADSL* enzymatic kinetic by isothermal titration calorimetry.

Keywords: *Schistosoma mansoni*, purine salvage pathway, adenylosuccinate lyase

1. Introduction

Schistosomiasis is one of the most prevalent neglected tropical diseases and is ranked second only to malaria in global health importance. Estimates show that at least 218 million people required preventive treatment for schistosomiasis in 2015 [1]. The causative agents of human schistosomiasis are parasitic trematodes of the genus *Schistosoma*, of which *S. mansoni* is the only species found in South and Central America.

The purine salvage pathway was studied in schistosomes and schistosomules of *S. mansoni* in the 1970s and 1980s by Senft [2-9] and Dovey [10], who demonstrated that the parasite do not have *de novo* purine synthesis pathway and therefore purine salvage pathway is exclusively used to supply purine bases for energy requirements and nucleic acid synthesis.

Using *S. mansoni* extracts, Senft and co-workers revealed that more than a half of the labeled adenosine is converted to AMP by the indirect pathway (adenosine → inosine → hypoxanthine → IMP → AMP) using the enzymes: adenosine deaminase

(ADA), purine nucleoside phosphorylase (PNP), hypoxanthine-guanine phosphoribosyltransferase (HGPRT), adenylosuccinate synthase (ADSS) and adenylosuccinate lyase (ADSL). This was the first time that adenylosuccinate lyase activity was reported in the parasite. Additionally in the presence of PRPP, a considerable fraction of adenosine was converted to AMP by the actions of adenosine phosphorylase (AP) and adenine phosphoribosyltransferase (APRT). Thus, the direct conversion of adenosine to AMP through adenosine kinase activity accounts only for only for a small fraction of the adenosine metabolism [6].

Adenylosuccinate lyase (ADSL) is a bifunctional enzyme acting both in the *de novo* purine synthesis and the purine nucleotide salvage pathway. It catalyzes two non-sequential reactions: the conversion of 5-aminoimidazole-(N-succinylcarboxamide) ribonucleotide (SAICAR) into 5-aminoimidazole-4-carboxamide ribonucleotide (AICAR) in the *de novo* purine biosynthetic pathway and the cleavage of adenylosuccinate (ADS) into adenosine 5'-monophosphate (AMP) and fumarate [11] in the purine salvage pathway. However, both reactions feature the β -elimination of fumarate, enzymes that catalyze this type of reaction belong to the β -elimination superfamily, the members of which are all homotetramers [12].

Adenylosuccinate lyase plays an integral part in maintaining proper cellular metabolism. In humans, ADSL mutations can have severe clinical consequences, ranging from a fatal neonatal form, to the Type I form which is characterized by severe psychomotor retardation, microcephaly, seizures and autistic features, to the more moderate type II form which is more slowly progressing but is still characterized by a degree of psychomotor retardation [13, 14].

In 2002, Foulk et al. [15] performed a detailed analysis of gene structure, mRNA expression, and analysis of the predicted protein structure of *S. mansoni* ADSL.

Expression levels of the ADSL, HGPRT and APRT enzymes were compared in different stages of the parasite life cycle: cercariae, schistosomula, and adult male and female. The levels of ADSL and HGPRT are lower in schistosomules and cercariae than in the adult worms and APRT levels seem fairly consistent in each stage of the life cycle. ADSL seems to be up regulated in mature worms when compared to the other stages of the life cycle examined. The level of mRNA expression is higher in females, with an ADSL activity 2.5 times higher than males. This could indicate that females needed a higher level of nucleotides for DNA synthesis necessary for egg laying and/or the branch of purine salvage pathway, which utilizes ADSL enzyme, is more active, making females more ADSL dependent than males.

In the present study, we describe the *Sm*ADSL production, enzyme kinetics, crystallization and structure determination of *Sm*ADSL in APO form and in complex with AMP, highlighting our efforts to obtain full kinetic and structural information for this important metabolic pathway. Indeed, there are six more structures from the purine salvage pathway solved in our group: purine nucleoside phosphorylase isoform 1 [16-19], adenosine kinase [20], adenylate kinase [21], methylthioadenosine phosphorylase [22], purine nucleoside phosphorylase isoform 2 (in press) and hypoxanthine-guanine phosphoribosyltransferase (in press). The description of the structure and kinetics of these enzymes permits a better understanding of the context of the metabolism of nucleotides in *S. mansoni* and represents another layer of structural and kinetic knowledge for the purine salvage pathway.

2. Materials and methods

2.1 Cloning, expression and purification of *Sm*ADSL

The coding sequence for *SmADSL* was obtained by searching the *S. mansoni* genome project database (<http://www.genedb.org/Homepage/Smansoni>; code Smp_038030). The *SmADSL* gene was synthesized by GenScript company.

Forward (5'-AAGTTCTGTTTCAGGGCCCGGACGAATTTGAAGAATACCGTAACCCGC-3') and reverse (5'-ATGGTCTAGAAAGCTTTAGATCGTAATATTAGAGTTCAGAGCCAGACAGTC-3')

primers were designed in order to amplify the *SmADSL* cDNA. This was then amplified by PCR using *PhusionTM Flash High-Fidelity*. An amplification product was treated with 10 U of DpnI and purified using AMPure magnetics-bead (BeckmanCoulter), 3 µL of amplification product and 1 µL (~100 ng) of the appropriately linearized pOPIN (pOPINS3C, pOPINTRX, pOPINE, pOPINM, and pOPINF), plus 6 µL of water were mixed in the wells of an In-FusionTM Dry-Down 96-well plate and incubated at 42°C for 30 min. All reactions were diluted 1:5 with T.E. Buffer (10 mM Tris pH 8.0, 1 mM EDTA) and 5 µL used to transform OmniMaxII T1-phage resistant cells (Invitrogen) in 96-tube format. Transformants were selected by plating on 24-well culture plates containing 1 ml of LB Agar/well, supplemented with the carbenicillin (50 mg/ml)/0.02% w/v X-Gal and 1 mM IPTG, and incubation overnight at 37 °C, as described by Berrow et al. 2007 [23, 24]. We selected the following pOPIN vectors: pOPINTRX, pOPINF, pOPINE, pOPINS3C and pOPINM.

LB medium (1.2 mL) was inoculated with white colonies (two per vector) supplemented with carbenicillin (50 mg/ml) in deep wells plates, after growing 16 hours at 200 rpm, the cells were harvested by centrifugation, and bacteria pellets were used for plasmid extraction using QIAgen BioRobot 8000 and QIAgen Turboprep kits. The content of each plasmid was checked by PCR using T7F and specific reverse primer. The purified plasmid was transformed into *Escherichia coli* Lemo21(DE3). Cells

transformants with this plasmid were selected on LB agar plates containing carbenicillin (50 mg/ml) and chloramphenicol (35 mg/mL), 20% X-Gal and 0,5 mM IPTG.

Positives colonies were inoculated in LB medium and shaken overnight at 37 °C. Expression was performed PowerBrothTM medium supplemented with carbenicillin (50 mg/ml) and chloramphenicol (35 mg/mL), inoculated with 1:100 of overnight culture and grown to an OD₆₀₀ of 0.6 at 37 °C. The expression was induced by the addition of 1 mM IPTG (isopropyl β-d-1-thiogalactopyranoside) and allowed to proceed overnight at 20 °C. The cells were centrifuged at 4000 g for 40 min at 4 °C, suspended (3 mL: 1 g pellet) in lysis buffer (50 mM Tris-HCl pH 7.5, 500 mM NaCl, 30 mM imidazole, 1mM MgCl₂ and 5mM β-mercaptoethanol). The cells were lysed using a 6 min sonication and centrifuged at 13000 g for 30 min at 4 °C.

SmADSL in the soluble fraction was purified using Talon Cobalt affinity column. The column was washed with 10 column volumes using lysis buffer. The *SmADSL* was eluted using elution buffer (50 mM Tris-HCl pH 7.5, 500 mM NaCl, 500 mM imidazole, 1mM MgCl₂ and 5mM β-mercaptoethanol). The purification steps were analyzed by SDS-PAGE. The purified *SmADSL* was dialyzed against 50 mM Tris-HCl pH 7.5, 500 mM NaCl, 1mM MgCl₂, 5 mM β-mercaptoethanol and 5% glycerol and concentrated to 5 mg/ml. The concentration was determined using NanoDrop spectrophotometer [25]. The dynamic light scattering (DLS) was performed as described by Lorber et al. 2012 [26] was used to provide the biologically oligomeric state/quaternary structure information. The dialyzed *SmADSL* was incubated with 5 mM AMP prior to crystallization screenings.

2.2 Enzyme Assays and Kinetic Studies

To investigate the *SmADSL* enzymatic kinetic, isothermal titration calorimetry (ITC) experiments were implemented as previously described [27] and the titration experiments were carried out using a VP-ITC calorimeter [28].

The *SmADSL* enzyme has two different substrates: ADS or SAICAR. Initially, a single injection methodology was performed to determine the apparent molar enthalpy (ΔH_{app}). 500 nM *SmADSL* were prepared in 20 mM NaH_2PO_4 , 200 mM NaCl and 1 mM MgCl_2 buffer and placed in microcalorimeter cell of the isothermal titration VP-ITC (Microcal) at 25 °C. In the syringe, 300 μL of ADS (1 mM) were filled using the same buffer. To proceed with the ΔH_{app} determination, a single injection with 20 μL of substrate was used and the heat exchange monitored for 1200 seconds. After subtracting the ADS heat dilution, the apparent molar enthalpy (ΔH_{app}) was obtained. The same procedure was used in the SAICAR reaction using 11.2 μM in syringe. This assay was also applied to measure the products (AMP + Fumarate and AICAR + Fumarate) heat exchange in order to check the enzyme activity against these molecules where 1 mM of substrate were charged in syringe with the same concentration of the respective combination, such as, AMP and Fumarate at the same concentration and after AICAR and Fumarate. During the injection, one of them was still kept at the same concentration inside the cell (1 mM) in order to not influence the measurements.

To follow the kinetic behavior of ADS, the syringe was filled with 1 mM ADS and the sample cell was filled with 50 nM of the *SmADSL* enzyme using the same buffer as previously described. The substrate was titrated with 17 injections (4 μL each). To analyze the second substrate, 18 injections of 4 μL of SAICAR (11.2 μM) were titrated using the same conditions as previously established. These experiments were carried out at 25 °C and a stirring speed of 300 rpm. The Michaelis-Menten fit was obtained by one substrate model. The estimates were calculated based on the

relationship between V_{max} and K_M for the sample in the presence and absence of inhibitor. The results were processed using Origin 7.0 software, which was included with the microcalorimeter, and the integral of the curve obtained reflects the heat variation in the system.

2.3 Crystallization and data collection

Initial crystallization trials were performed at the OPPF-UK, with the sitting-drop vapor-diffusion method in Greiner 96 well plates using crystallization kits Wizard 1 and 2 (Rigaku), Morpheus, JCSG+ (Molecular Dimensions) and Index (Hampton Research). A pre-Crystallization Test (Hampton Research) was employed to determine the optimal concentrations of protein for crystallization. The actual crystallization assays were done using Hydra and Cartesian robots dispensing 100nL drops of 5 mg/mL *SmADSL*. Plates were stored in Formulatrix imaging systems at 18 °C. *SmADSL* crystallized in several conditions of the Morpheus crystallization kit [29].

Several crystals were screened with x-rays and one dataset of *SmADSL* in complex with AMP was collected for a crystal grown in condition E12 (30mM of each diethyleneglycol, triethyleneglycol, tetraethyleneglycol, pentaethyleneglycol; 100mM of Tris/bicine pH8.5; 12.5% of MPD, PEG1000 and PEG3350), on beamline I02 ($\lambda=0.9795$) at Diamond Light Source (DLS) up to 2.36 Å resolution. Crystals of *SmADSL* in APO form were obtained in condition F2 of Morpheus kit which consists in 10% PEG8000, 20% ethyleneglycol, 20mM of each D-glucose, D-mannose, D-galactose, L-fucose, D-xylose, *N*-acetyl-D-glucosamine; 100 mM MES/Imidazole pH 6.5. Datasets were obtained on beamline I04-1 at DLS using $\lambda=0.9200$, up to 2.14 Å resolution. Data were processed automatically using Xia2 [30], XDS [31], CCP4 [32]

and aimless [33] software. Table 1 shows the statistics of data collection processing and refinement.

2.4 Structure resolution and refinement

The *SmADSL*-AMP complex was solved by molecular replacement using human ADSL-AMP complex (PDB ID 2J91) as the search model. The model shares approximately 57% sequence identity to *SmADSL*. One molecule was located per asymmetric unit, using the Phaser program [34]. Refinement was performed in Phenix [35] alternated with inspection of Fourier synthesis (2Fo - Fc and Fo - Fc) electron density maps and model manipulation together with ligand incorporation using Coot [36]. MolProbity [37] was used to investigate model geometry in combination with the validation tools provided in Coot. The *SmADSL* Apo structure was also solved by Phaser employing the refined *SmADSL*-AMP complex as search model. Refinement was also performed with Phenix/Coot cycles using XYZ coordinates, individual B-factors, TLS and weight optimization parameters. Figures were prepared with PyMOL [38]. Amino-acid sequence alignments were carried out using the program ClustalX [39].

3. Results and Discussion

3.1 Expression, purification and sequence analysis

The *SmADSL* gene (Smp_038030) codes for a protein with 480 amino acids (calculated MW of 54501.2 Da) which shares 56.4% of identity with human ADSL. Its

coding region was cloned into pOPIN vectors using OPPF-UK facilities and small scale expression trials were used to identify the vector and induction conditions resulting in the highest predicted protein yield. The pOPINF (6His-Tag in N-terminus) construct was identified as being the best, and following scale up and purification, ~15 mg of recombinant protein per liter of Power Broth. The protein was readily purified in a single step using Talon resin.

3.2 Enzyme Assays and Kinetic Studies

The *SmADSL* enzymatic activity was determined using Isothermal Titration Calorimetry (ITC) assays revealing an endothermic reaction with enthalpy exchange reaction of $\Delta H_{ADS} = +8.9$ kcal/mol and $\Delta H_{SAICAR} = +4.7$ kcal/mol (Fig. 1) obtained by single injection in saturating conditions. The ΔH of > 0 indicates an endothermic reaction where the entropy contribution must be important to the kinetic reaction to produce $\Delta G < 0$. The high entropy contribution is related to large quantities of water molecules observed in the structure of the active site (about forty molecules, Fig. 2).

Single injection ITC was also used to verify if *SmADSL* conversion of ADS or SAICAR to AMP/Fumarate and AICAR/Fumarate, respectively, is irreversible. This was shown by apparent molar enthalpy determination of a ITC mixing *SmADSL* with AMP/Fumarate or AICAR/Fumarate, which resulted in heat values close to the dilution values previously measured under the same experimental conditions ($\Delta H \sim 0$ kcal/mol) (data not shown), therefore, there is no enzymatic activity to either AMP/Fumarate or AICAR/Fumarate.

Multiple injection methodology was performed to determine the enzyme kinetic activity with respect to substrate concentration for both ADS and SAICAR, these

data were fitted to the Michaelis-Menten equation using a single binding site model and the kinetic parameters for ADS were $K_M = (17.2 \pm 2.3) \mu\text{M}$ and $k_{\text{cat}} = (0.73 \pm 0.04) \text{ s}^{-1}$ and for SAICAR $K_M = (5.27 \pm 1.2) \mu\text{M}$ and $k_{\text{cat}} = (1.8 \pm 0.3) \text{ s}^{-1}$ (Table 2). The BRENDA data base does not have any values of this enzyme in *Schistosoma sp.*

In comparison to human ADSL (*HsADSL*), the *SmADSL* ADS K_M is 10 times higher ($1.46 \mu\text{M}$ for the human enzyme) and is more similar to the *Bacillus subtilis* mutants (*BsADSL*) on residues I62D and D69E, which changes the wild type ADS K_M values from $2.1 \mu\text{M}$ to $17.7 \mu\text{M}$. The k_{cat} value is unique, the closest match is *BsADSL* mutant S94A (1.14 s^{-1}). The only wild-type enzyme that presents tabled k_{cat} values is the *BsADSL* (1.74 s^{-1}). The low k_{cat}/K_M value ($0.042 \pm 0.006 \mu\text{M}^{-1} \text{ s}^{-1}$) for *BsADSL* reflects the high efficiency to ADS consumption is not comparable to any other value described to this enzyme at BRENDA database.

The reported SAICAR K_M value for *HsADSL* ($1.74 \mu\text{M}$) is close to the *SmADSL* value to this substrate. Unfortunately, due to a lack of characterization of this substrate in the literature to a comparison of its enzymatic properties cannot be carried out.

The BRENDA data base does not contains k_{cat} values for *HsADSL* and the SAICAR substrate that, consequently, cannot provide k_{cat}/K_M relation and consequently, not allowing the comparison between the *SmADSL* k_{cat}/K_M value ($0.3 \pm 0.1 \mu\text{M}^{-1} \text{ s}^{-1}$). Is worth emphasizing that, the ADS and SAICAR concentration values in bloodstream are unknown, according to the Human metabolomics database (HMDB), which suggests that there is a low concentration of these metabolites indicating the necessity of the highly efficient *SmADSL* enzyme to be able to use these substrates, preferring the ADS produced by Adenylosuccinate synthase (ADSS). Some differences in kinetics

parameters values can be explained by using different methodologies, since the ITC assays depend on the enthalpy variation during enzymatic activity.

3.3 *SmADSL* Structure description

SmADSL crystallizes in an orthorhombic system and the systematic absences together with symmetry operators indicated space group *I*222 to *SmADSL*-AMP and *P*2₁2₁2 to *SmADSL*-Apo, with a single polypeptide chain, labelled chain A in asymmetric unit for the former and two polypeptides chains labelled chain A and chain B for the latter. The crystallographic statistics and model geometry (Table 1) indicate the analysis has produced an acceptable medium resolution model. AMP, a product of the catalyzed reaction, was present in the crystallization condition and a well-defined electron density for the ligand was observed in the active site.

The refinement was completed using programs Phenix and Coot for values R and R_{Free} of 19.16 and 23.12%, respectively, for the *SmADSL*-AMP and $R_{\text{work}} = 22.24\%$ e $R_{\text{free}} = 25.57\%$ for the *SmADSL* Apo form. The coordinates and structure-factor data have been deposited in the Protein Data Bank with accession codes 5EYT (*ADSL*-AMP) and 5EYV (*ADSL*-Apo).

The global structure consists almost entirely of α -helices with only 2 β -strands. This is the only enzyme in the purine salvage pathway to catalyze two separate reactions, both catalyzed by adenylosuccinate lyase and involve the β -elimination of fumarate. Enzymes that catalyze this type of reaction belong to a superfamily, the members of which are homotetramers. Similar to other enzymes in the beta-elimination superfamily, the *SmADSL* monomer can be divided into three domains that combine to form an elongated structure (Fig. 3). Domains I and III are placed at either end of the

long helical bundle formed by domain II. Domain I comprises residues 1 – 101, which form six helices ($\alpha 1 - \alpha 7$). Domain II, consisting of residues 102 – 358, forms an elongated helical bundle assembled by $\alpha 8$ through $\alpha 15$ as well as a short two-stranded antiparallel β -sheet ($\beta 1, \beta 2$) positioned between $\alpha 8$ and $\alpha 9$. The domain III comprises nine helices ($\alpha 16 - \alpha 25$) constructed from residues 359 – 480. Furthermore, the domain II carries unresolved portion of the structure: residues $^{281}\text{QIGSSA}^{286}$ (*SmADSL*-AMP) and $^{281}\text{QIGSSAMPY}^{289}$ (*SmADSL*-Apo) are on a disordered loop. This loop contains the signature sequence $^{281}\text{Q}^*\text{GSS}^*\text{MP}^*\text{K}^*\text{NP}^{293}$ unique to the β -elimination superfamily [12]. This sequence is the same in *SmADSL* and human ADL ($^{281}\text{QIGSSAMPYKRNP}^{293}$). Comparison of the translated *SmADSL* peptide sequence with all adenylosuccinate lyases from PDB indicate five residues (Ala157, Gly198, Pro288, Lys290 and Asn292) that are conserved between them.

Dynamic light scattering (DLS) indicates that *SmADSL* (at 1 mg/mL) exists as a two species in solution, suggesting the presence of a dimer (8%) and tetramer (92%) under the conditions used during the final stage of purification (data not shown). Changes in the multimeric state of *SmADSL* orthologues have been reported elsewhere. The *B. subtilis* orthologue enzyme has been shown to exist largely as a dimeric species when the protein concentration is low (0.1 mg/ml); however, as the protein concentration increases the tetrameric species becomes the most abundant form [40]. Crystallographic structures of orthologues also revealed the formation of tetramers (Fig. 4). This oligomeric state is necessary for the function of the enzyme [41-43].

Quantitative comparison of three-dimensional structures to determine structural similarity between *SmADSL*-AMP (chain A) and *SmADSL*-Apo (chain A and B) the RMSd value is 1.3 Å to chain A and 0.28 Å to chain B. The RMSd value for tetramers superposition is 1.14 Å. The most significant difference between them is in domain III

where the orientation is different in *SmADSL*-Apo chain A and partial disordered in chain B. *SmADSL*-Apo chain B carries unresolved portion of the structure: residues 391-435.

The fold is highly similar between *SmADSL* and *HsADSL*. Quantitative comparison of three-dimensional structures between them has RMSd value 1.43 Å to *SmADSL*-AMP/*HsADSL* and 1.46 Å to *SmADSL*-Apo/*HsADSL*. We see in common with other members of the β -elimination superfamily that *SmADSL* has a core structure composed of domain II that is highly conserved while domains I and III may change significantly, we see a difference in domain III orientation in comparison to the human enzyme [12]. The high level conservation of the fold in all ADSLs demonstrates that is important to enzymatic mechanism.

3.3.1 Active site

The tetramer contains four active sites. Interestingly, three monomers contribute to each of the four active sites in the tetramer. In the structure of *SmADSL*-AMP the AMP phosphate accepts hydrogen bonds from Arg14C, Tyr15C, Arg298C, Ser329A, Arg333A and water. The ribose O2 donates a hydrogen bond to the Arg79A carbonyl and O3 accepts hydrogen bonds from the carbonyl of Arg79A, Asp81A NH2 and water. The adenine N1 accepts a hydrogen bond from Ser106A and water; N6 donates hydrogen bonds to Gln236A (Fig. 5). The AMP binding site is totally conserved between the human ADSL and *SmADSL*. The conformation of the side chains is very similar between structures in complex with AMP, however in the Apo structure the side chain conformation of Arg79 and His80 is slightly different. A high degree of conservation around the active binding site is observed in all ADSLs, suggesting that

the enzymatic mechanism is strictly maintained. ADSL catalyzes a β -elimination that is thought to occur via a general acid–base uni–bi mechanism [44, 45]. However, the identification of the ADSL catalytic base has been subject to an extensive debate [40, 42, 46-49].

The loop comprising of amino acids 281-293 which is conserved in ADSL sequences is positioned surrounding in the active site between α -helices 12 and 13. Fyfe and collaborators [42] described this region in *Staphylococcus aureus* ADSL as a mobile loop, since the electron density in this region also is diffuse. In *E.coli* ADSL, this loop is disordered in the Apo form structure, but the presence of a ligand induces partial reorganization of the loop to near the binding site [47]. Such as *EcADSL* structure, in *SmADSL*-Apo this loop is more diffuse than *SmADSL*-AMP suggesting that the presence of the ligand generates loop stability. In the *SmADSL*-AMP structure, the side chain of Arg291 is down and away from the active site while the *SmADSL*-Apo structure the side chain of Arg291 is into the active site. In *SmADSL*-AMP, Lys290 moves away from the active site than in ADSL-Apo structure (Fig. 6). These differences suggests there is adaptation of the loop to the binder volume in the active site.

3.3.2 Dimer interface and structural stability

Fyfe *et al.* [42], during studies with ADSL of *Staphylococcus aureus* in complex with AMP, were intrigued by two observations. First, a tetramer (or dimer of dimers) is required to produce a functional enzyme since three subunits are required to contribute residues to form an active site. Second, there is less sequence conservation amongst the ADSL residues involved in the assembly of the quaternary structure than those around the active sites. Thus the dimer interface as a potential target for screening and

structure-based drug discovery methods was suggested by the authors. It is interesting because human ADSL deficiency is a selectively neuronopathic disorder with psychomotor retardation and epilepsy as leading traits [11]. Many different missense mutations in the human adenylosuccinate lyase deficient have been described and some of these mutations influence the stability of the tetramer [49]. In order to investigate the structure of *SmADSL* and how closely it resembles the human enzyme, Foulk [15] compared the residues of the human enzyme that, when mutated, inactivate the enzyme to the corresponding residue in the *S. mansoni* sequence (Table 3). Among these, schistosome residues Met20, Pro94, Arg135, Lys241, Arg298, and Ser434 are conserved with the corresponding normal human amino acid. Basic arginine residues at positions 190 and 426 of the normal human sequence occur as similar, basic lysine residues at positions 184 and 422 in *SmADSL*. The mutations that cause adenylosuccinate lyase deficiency in humans, there are two residues in *SmADSL* that are not conserved with respect to the nature of the amino acid side chain. Ala390 in *SmADSL* is hydrophobic, whereas this residue is a conserved polar residue in human, chicken, mouse, *B. subtilis* and *T. maritima* [49]. Also, a small, polar serine at position 418 of *SmADSL* is not consistent with the acidic aspartate residue that is conserved among the chicken, mouse and human enzymes [49], the side chain of Ser418 forms hydrogen bond with Glu209 and a water molecule in *SmADSL*. Interestingly, the schistosome enzyme possesses a valine at position 66, which is the same amino acid found in a mutant human enzyme. These differences suggest that these residues may be less important to the structure and function [15].

The mutation of Lys246 (Lys241 in *SmADSL*) for glutamic acid is located in the dimeric interface A-B or C- D and results in a predominantly monomeric protein with negligible enzymatic activity [50]. In the *SmADSL* structure, Lys241 residue of the

chain A makes a hydrogen bond with Thr256, two hydrogen bonds with Asp176 and two hydrogen bonds with Asn252 of chain B.

The mutation of Arg303 (Arg298 in *SmADSL*) to cysteine is located at B-C interface or the A-D interface in the formation of the tetramer. The importance of the equivalent residue in tetrameric stability and enzyme activity in *Bacillus subtilis* ADSL was demonstrated by site-directed mutagenesis experiments [40]. Subsequently, Ray and collaborators [51] carried thermodynamic and enzymatic studies of this mutation in human ADSL and observed loss of cooperativity between the three monomers that comprise the active site due the Arg303Cys mutation remove H-bonds between subunits. Interestingly, they found that unlike other mutations leading to deficiency ADSL, this mutation significantly affected the enzyme's ability to catalyze the conversion of ADS than SAICAR to respective products. In the *SmADSL* structure, the residue Arg298 of chain B interacts with the chain C mediated by a hydrogen bond with the residue Ile480B connected to a water molecule of chain C, which Glu75C also connects. The Glu75C makes a hydrogen bond with the Arg14B residue, which binds to the same molecule of water.

Other mutations, which are not found in the dimeric or tetrameric interface, are reported as important in the structural stability of the enzyme. Polenchar [40, 52] conducted site-directed mutagenesis experiments in *Bacillus subtilis* ADSL corresponding to the three described mutations (Met26Leu, Arg141Trp, Ser395Arg) for severe ADSL deficiency in humans (Table 3). These studies demonstrated the importance of these residues in the stability of the quaternary structure of the enzyme.

Targeting transient protein–protein interactions or the interface of oligomeric assemblies by screening and structure-based methods to find small molecule drug-like inhibitors presents a significant challenge [53]. Complicating factors include the high

degree of specificity and the large areas of interactions involved in complex formation. Nevertheless, *SmADSL* occurs in both dimeric and tetrameric forms, where the enzymatic activity lies only in the latter. Preventing the formation and/or destabilizing the tetramer could provide a route to enzyme inhibition [53]. It is important to remember that *HsADSL* is involved in two different reactions in the pathway of purine synthesis and purine salvage: the elimination of fumarate from SAICAR and ADS respectively. In contrast, in *Schistosoma* only the purine salvage pathway is active, so the *SmADSL* is involved mainly in adenylosuccinate conversion to AMP due the absence of SAICAR substrate in *S. mansoni*. These different biochemical functions may have resulted from the evolution of structural differences between parasite and host. Thus, these differences can lead to development of anti-schistosomiasis drugs based on selective inhibition of *SmADSL* [15].

4. Conclusions

The *SmADSL* structure was solved in Apo form and in complex with AMP in the active site. The *SmADSL* displays a fold and tetrameric structure conserved with orthologous enzymes. This oligomerization state is required since the active sites are comprised of residues from three of the four subunits. The active sites are highly conserved between species and it is difficult to identify a potent species-specific inhibitor for the development of new therapeutic agents. In contrast, several studies have demonstrated the importance of dimeric interface residues in the stability of the quaternary structure of the enzyme. Thus it may represent a potential target for which inhibitors might be developed. Interestingly, unlike other mutations leading to deficient ADSL in human, the Arg303Cys mutation further significantly affect the enzyme's

ability to catalyze the conversion of ADS more than SAICAR to respective products. It is important to remember that human ADSL is involved in two different reactions in the pathway of purine synthesis and purine salvage: the elimination of fumarate from SAICAR and ADS respectively. In contrast, in *Schistosoma*, only the purine salvage pathway is active, so the *SmADSL* is involved only in adenylosuccinate conversion to AMP. These different biochemical functions may have resulted in the evolution of structural differences between parasite and host. Thus, these differences can lead to development of anti-schistosomiasis drugs based on inhibition selective to *SmADSL*. The *SmADSL* enzymatic activity assay showed an endothermic reaction, indicating the contribution of the entropy related to the large quantity of water molecules present in the active site is important for the reaction kinetics. The description of the structure and kinetics of this ADSL enzyme allow a better understanding of the context of the metabolism of adenine nucleotides in *S. mansoni* and represent another layer of structural and kinetic knowledge on the purine salvage pathway. Indeed, there are six other structures solved in our group for purine salvage pathway enzymes: purine nucleoside phosphorylase isoform 1 and isoform 2, adenosine kinase, adenylylate kinase, hypoxanthine-guanine phosphoribosyltransferase and methylthioadenosine phosphorylase, highlighting our efforts to obtain full kinetic and structural information for this important metabolic pathway.

Acknowledgements

We acknowledge the Fundação de Amparo a Pesquisa do Estado de São Paulo (FAPESP) grants 2012/05532-8 (LR) 2012/14223-9 (HMP) 2012/23730-1 (VHBS) and

CNPq grant 474402/2013-4 and 140636/2013-7 for financial support, Oxford Protein Production Facility (OPPF-UK) and Diamond Light Source (DLS-UK).

References

- [1] WHO. Schistosomiasis and soil-transmitted helminthiasis: number of people treated in 2015. *Wkly Epidemiol Rec.* 2016;91:585-95.
- [2] Miech FP, Senft AW, Senft DG. Pathways of nucleotide metabolism in *Schistosoma mansoni*--VI adenosine phosphorylase. *Biochemical pharmacology.* 1975;24:407-11.
- [3] Senft AW, Crabtree GW. Pathways of nucleotide metabolism in *Schistosoma mansoni*--VII. Inhibition of adenine and guanine nucleotide synthesis by purine analogs in intact worms. *Biochemical pharmacology.* 1977;26:1847-55.
- [4] Senft AW, Crabtree GW. Purine metabolism in the schistosomes: potential targets for chemotherapy. *Pharmacology & therapeutics.* 1983;20:341-56.
- [5] Senft AW, Miech RP, Brown PR, Senft DG. Purine metabolism in *Schistosoma mansoni*. *International journal for parasitology.* 1972;2:249-60.
- [6] Senft AW, Crabtree GW, Agarwal KC, Scholar EM, Agarwal RP, Parks RE, Jr. Pathways of nucleotide metabolism in *Schistosoma mansoni*. 3. Identification of enzymes in cell-free extracts. *Biochemical pharmacology.* 1973;22:449-58.
- [7] Senft AW, Senft DG, Miech RP. Pathways of nucleotide metabolism in *Schistosoma mansoni*. II. Disposition of adenosine by whole worms. *Biochemical pharmacology.* 1973;22:437-47.
- [8] Stegman RJ, Senft AW, Brown PR, Parks RE, Jr. Pathways of nucleotide metabolism in *Schistosoma mansoni*. IV. Incorporation of adenosine analogs in vitro. *Biochemical pharmacology.* 1973;22:459-68.
- [9] Crabtree GW, Senft AW. Pathways of nucleotide metabolism in *Schistosoma mansoni*. V. Adenosine cleavage enzyme and effects of purine analogues on adenosine metabolism in vitro. *Biochemical pharmacology.* 1974;23:649-60.
- [10] Dovey HF, McKerrow JH, Wang CC. Purine salvage in *Schistosoma mansoni* schistosomules. *Molecular and biochemical parasitology.* 1984;11:157-67.
- [11] Kmoch S, Hartmannova H, Stiburkova B, Krijt J, Zikanova M, Sebesta I. Human adenylosuccinate lyase (ADSL), cloning and characterization of full-length cDNA and its isoform, gene structure and molecular basis for ADSL deficiency in six patients. *Human molecular genetics.* 2000;9:1501-13.
- [12] Toth EA, Yeates TO. The structure of adenylosuccinate lyase, an enzyme with dual activity in the de novo purine biosynthetic pathway. *Structure.* 2000;8:163-74.
- [13] Jurecka A, Tytki-Szymanska A, Zikanova M, Krijt J, Kmoch S. D-ribose therapy in four Polish patients with adenylosuccinate lyase deficiency: absence of positive effect. *J Inherit Metab Dis.* 2008;31 Suppl 2:S329-32.
- [14] Jurecka A, Zikanova M, Tytki-Szymanska A, Krijt J, Bogdanska A, Gradowska W, et al. Clinical, biochemical and molecular findings in seven Polish patients with adenylosuccinate lyase deficiency. *Molecular genetics and metabolism.* 2008;94:435-42.
- [15] Foulk BW, Pappas G, Hirai Y, Hirai H, Williams DL. Adenylosuccinate lyase of *Schistosoma mansoni*: gene structure, mRNA expression, and analysis of the predicted peptide structure of a potential chemotherapeutic target. *International journal for parasitology.* 2002;32:1487-95.
- [16] Pereira HD, Franco GR, Cleasby A, Garratt RC. Structures for the potential drug target purine nucleoside phosphorylase from *Schistosoma mansoni* causal agent of schistosomiasis. *Journal of molecular biology.* 2005;353:584-99.

- [17] Pereira HM, Berdini V, Ferri MR, Cleasby A, Garratt RC. Crystal structure of *Schistosoma* purine nucleoside phosphorylase complexed with a novel monocyclic inhibitor. *Acta tropica*. 2010;114:97-102.
- [18] Pereira HM, Cleasby A, Pena SS, Franco GG, Garratt RC. Cloning, expression and preliminary crystallographic studies of the potential drug target purine nucleoside phosphorylase from *Schistosoma mansoni*. *Acta crystallographica Section D, Biological crystallography*. 2003;59:1096-9.
- [19] Pereira HM, Rezende MM, Castilho MS, Oliva G, Garratt RC. Adenosine binding to low-molecular-weight purine nucleoside phosphorylase: the structural basis for recognition based on its complex with the enzyme from *Schistosoma mansoni*. *Acta crystallographica Section D, Biological crystallography*. 2010;66:73-9.
- [20] Romanello L, Bachega JF, Cassago A, Brandao-Neto J, DeMarco R, Garratt RC, et al. Adenosine kinase from *Schistosoma mansoni*: structural basis for the differential incorporation of nucleoside analogues. *Acta crystallographica Section D, Biological crystallography*. 2013;69:126-36.
- [21] Marques Ide A, Romanello L, DeMarco R, Pereira HD. Structural and kinetic studies of *Schistosoma mansoni* adenylate kinases. *Molecular and biochemical parasitology*. 2012;185:157-60.
- [22] Torini JR, Brandao-Neto J, DeMarco R, Pereira HD. Crystal Structure of *Schistosoma mansoni* Adenosine Phosphorylase/5'-Methylthioadenosine Phosphorylase and Its Importance on Adenosine Salvage Pathway. *PLoS neglected tropical diseases*. 2016;10:e0005178.
- [23] Berrow NS, Alderton D, Sainsbury S, Nettleship J, Assenberg R, Rahman N, et al. A versatile ligation-independent cloning method suitable for high-throughput expression screening applications. *Nucleic acids research*. 2007;35:e45.
- [24] Bird LE. High throughput construction and small scale expression screening of multi-tag vectors in *Escherichia coli*. *Methods*. 2011;55:29-37.
- [25] Desjardins P, Hansen JB, Allen M. Microvolume protein concentration determination using the NanoDrop 2000c spectrophotometer. *J Vis Exp*. 2009.
- [26] Lorber B, Fischer F, Bailly M, Roy H, Kern D. Protein analysis by dynamic light scattering: methods and techniques for students. *Biochem Mol Biol Educ*. 2012;40:372-82.
- [27] Todd MJ, Gomez J. Enzyme kinetics determined using calorimetry: a general assay for enzyme activity? *Anal Biochem*. 2001;296:179-87.
- [28] Wiseman T, Williston S, Brandts JF, Lin LN. Rapid measurement of binding constants and heats of binding using a new titration calorimeter. *Anal Biochem*. 1989;179:131-7.
- [29] Gorrec F. The MORPHEUS protein crystallization screen. *Journal of applied crystallography*. 2009;42:1035-42.
- [30] Winter G, Lobley CM, Prince SM. Decision making in xia2. *Acta crystallographica Section D, Biological crystallography*. 2013;69:1260-73.
- [31] Kabsch W. Xds. *Acta crystallographica Section D, Biological crystallography*. 2010;66:125-32.
- [32] Winn MD, Ballard CC, Cowtan KD, Dodson EJ, Emsley P, Evans PR, et al. Overview of the CCP4 suite and current developments. *Acta crystallographica Section D, Biological crystallography*. 2011;67:235-42.
- [33] Evans P. Scaling and assessment of data quality. *Acta crystallographica Section D, Biological crystallography*. 2006;62:72-82.
- [34] McCoy AJ, Grosse-Kunstleve RW, Adams PD, Winn MD, Storoni LC, Read RJ. Phaser crystallographic software. *Journal of applied crystallography*. 2007;40:658-74.
- [35] Adams PD, Grosse-Kunstleve RW, Hung LW, Ioerger TR, McCoy AJ, Moriarty NW, et al. PHENIX: building new software for automated crystallographic structure determination. *Acta crystallographica Section D, Biological crystallography*. 2002;58:1948-54.
- [36] Emsley P, Cowtan K. Coot: model-building tools for molecular graphics. *Acta crystallographica Section D, Biological crystallography*. 2004;60:2126-32.

- [37] Chen VB, Arendall WB, 3rd, Headd JJ, Keedy DA, Immormino RM, Kapral GJ, et al. MolProbity: all-atom structure validation for macromolecular crystallography. *Acta crystallographica Section D, Biological crystallography*. 2010;66:12-21.
- [38] DeLANO WL. The PyMOL Molecular Graphics System. 2002.
- [39] Larkin MA, Blackshields G, Brown NP, Chenna R, McGettigan PA, McWilliam H, et al. Clustal W and Clustal X version 2.0. *Bioinformatics*. 2007;23:2947-8.
- [40] Palenchar JB, Colman RF. Characterization of a mutant *Bacillus subtilis* adenylosuccinate lyase equivalent to a mutant enzyme found in human adenylosuccinate lyase deficiency: asparagine 276 plays an important structural role. *Biochemistry*. 2003;42:1831-41.
- [41] Vedadi M, Lew J, Artz J, Amani M, Zhao Y, Dong A, et al. Genome-scale protein expression and structural biology of *Plasmodium falciparum* and related Apicomplexan organisms. *Molecular and biochemical parasitology*. 2007;151:100-10.
- [42] Fyfe PK, Dawson A, Hutchison MT, Cameron S, Hunter WN. Structure of *Staphylococcus aureus* adenylosuccinate lyase (PurB) and assessment of its potential as a target for structure-based inhibitor discovery. *Acta crystallographica Section D, Biological crystallography*. 2010;66:881-8.
- [43] Banerjee S, Agrawal MJ, Mishra D, Sharan S, Balaram H, Savithri HS, et al. Structural and kinetic studies on adenylosuccinate lyase from *Mycobacterium smegmatis* and *Mycobacterium tuberculosis* provide new insights on the catalytic residues of the enzyme. *FEBS J*. 2014;281:1642-58.
- [44] Bridger WA, Cohen LH. The kinetics of adenylosuccinate lyase. *The Journal of biological chemistry*. 1968;243:644-50.
- [45] Casey PJ, Lowenstein JM. Purification of adenylosuccinate lyase from rat skeletal muscle by a novel affinity column. Stabilization of the enzyme, and effects of anions and fluoro analogues of the substrate. *Biochem J*. 1987;246:263-9.
- [46] Toth EA, Worby C, Dixon JE, Goedken ER, Marqusee S, Yeates TO. The crystal structure of adenylosuccinate lyase from *Pyrobaculum aerophilum* reveals an intracellular protein with three disulfide bonds. *Journal of molecular biology*. 2000;301:433-50.
- [47] Tsai M, Koo J, Yip P, Colman RF, Segall ML, Howell PL. Substrate and product complexes of *Escherichia coli* adenylosuccinate lyase provide new insights into the enzymatic mechanism. *Journal of molecular biology*. 2007;370:541-54.
- [48] Bulusu V, Srinivasan B, Bopanna MP, Balaram H. Elucidation of the substrate specificity, kinetic and catalytic mechanism of adenylosuccinate lyase from *Plasmodium falciparum*. *Biochimica et biophysica acta*. 2009;1794:642-54.
- [49] Marie S, Cuppens H, Heuterspreute M, Jaspers M, Tola EZ, Gu XX, et al. Mutation analysis in adenylosuccinate lyase deficiency: eight novel mutations in the re-evaluated full ADSL coding sequence. *Hum Mutat*. 1999;13:197-202.
- [50] Ariyananda Lde Z, Lee P, Antonopoulos C, Colman RF. Biochemical and biophysical analysis of five disease-associated human adenylosuccinate lyase mutants. *Biochemistry*. 2009;48:5291-302.
- [51] Ray SP, Deaton MK, Capodagli GC, Calkins LA, Sawle L, Ghosh K, et al. Structural and biochemical characterization of human adenylosuccinate lyase (ADSL) and the R303C ADSL deficiency-associated mutation. *Biochemistry*. 2012;51:6701-13.
- [52] Palenchar JB, Crocco JM, Colman RF. The characterization of mutant *Bacillus subtilis* adenylosuccinate lyases corresponding to severe human adenylosuccinate lyase deficiencies. *Protein science : a publication of the Protein Society*. 2003;12:1694-705.
- [53] Yin H, Hamilton AD. Strategies for targeting protein-protein interactions with synthetic agents. *Angew Chem Int Ed Engl*. 2005;44:4130-63.
- [54] Lunin VY, Afonine PV, Urzhumtsev AG. Likelihood-based refinement. I. Irremovable model errors. *Acta Crystallogr A*. 2002;58:270-82.

644 Table 1 - Statistics of data collection processing and refinement.
645

Data Collection	ADSL - AMP	ADSL - APO
Space Group	<i>I</i> 222	<i>P</i> 2 ₁ 2 ₁ 2 ₁
Cell dimensions (Å) <i>a</i> , <i>b</i> , <i>c</i> .	70.50, 73.06, 180.35	76.16, 82.63, 163.78
Detector	PILATUS 6M	PILATUS 2M
X-ray source	DLS I02	DLS I04-1
Wavelength (Å)	0.9795	0.9200
Resolution range (Å)	35.23 - 2.36 (2.49 - 2.36)	58.16 - 2.14 (2.20 - 2.14)
Redundancy	5.4 (5.6)	7.2 (7.1)
<i>R</i> _{pim} (%)	6.2 (29.7)	5.2 (29.8)
CC (1/2)	0.987 (0.730)	0.996 (0.701)
Completeness(%)	99.8 (98.2)	99.8 (99.9)
Total reflections	105164 (15589)	414384 (29958)
Unique reflections	19416 (2774)	57766 (4219)
I/sigma (I)*	8.5 (2.6)	10.4 (2.6)
Refinement parameters		
Reflections used for refinement	19399	57730
<i>R</i> (%)	19.16	22.24
<i>R</i> _{Free} (%)	23.12	25.57
No. of protein atoms	3735	6871
No. of ligand atoms	23	-
B (Å ²)	32.6	30.0
Coordinate Error (ML based) (Å)	0.27	0.28
Phase error (°) [54]	23.58	24.85
Ramachandran Plot		
Favored (%)	92.8	91.0
Allowed (%)	7.1	9.0
Outliers (%)	-	-
All-atom Clashscore	5.83	5.24
RMSD from ideal geometry		
r.m.s. bond lengths (Å)	0.002	0.002
r.m.s. bond angles (°)	0.544	0.493
PDB ID	5EYT	5EYV

646 * I/sigma > 2 for useful data. Average intensity / average intensity error.

Table 2: Kinetic parameters: The mean value of enzymatic kinetic parameters to adenylosuccinate (ADS) and SAICAR, respectively, with standard deviations from biological triplicates.

ADS → AMP + Fumarate

	ΔH (cal/mol)	K_M (μM)	k_{cat} (s^{-1})	K_{cat}/K_M (μMs) $^{-1}$
ADS	9.0 ± 0.2	17.2 ± 2.3	0.73 ± 0.04	0.042 ± 0.006

SAICAR → AICAR + Fumarate

	ΔH (cal/mol)	K_M (μM)	k_{cat} (s^{-1})	K_{cat}/K_M (μMs) $^{-1}$
SAICAR	4.7 ± 1.3	5.3 ± 1.2	1.8 ± 0.3	0.3 ± 0.1

Table 3 - Comparison of selected *Schistosoma mansoni* adenylosuccinate lyase residues with corresponding residues from human wild type and mutant adenylosuccinate lyases.

ADSL human	ADSL human Mutant*	ADSL <i>Schistosoma mansoni</i>
Met26	Leu26	Met20
Ile72	Val72	Val66
Pro100	Ala100	Pro94
Arg141	Trp141	Arg135
Arg190	Gln190	Lys184
Lys246	Arg246	Lys241
Arg303	Cys303	Arg298
Ser395	Arg395	Ala390
Asp422	Tyr422	Ser418
Arg426	His426	Lys422
Ser438	Pro438	Ser434

Fonte: FOULK et al. [15]

*Missense mutations that cause adenylosuccinate lyase deficiency in humans. Mutations are described or reviewed in Marie et al., 1999 [47].

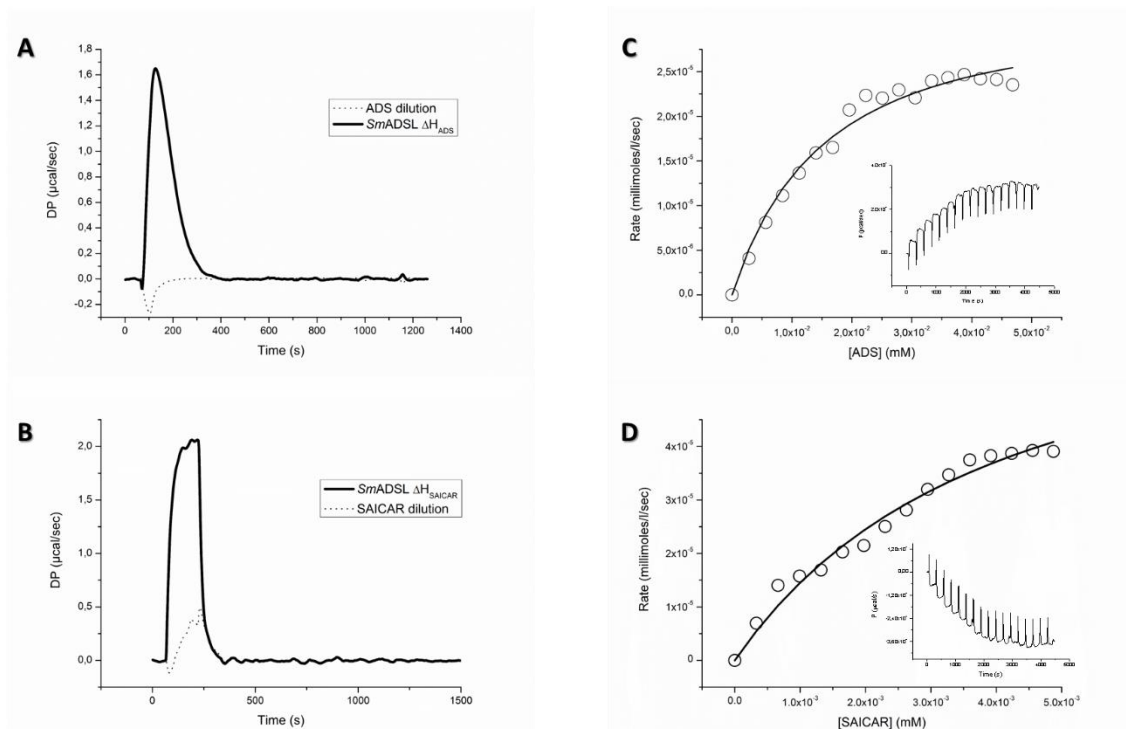


Figure 1. Enzyme assays. The apparent enthalpy variation (ΔH_{app}) obtained by single injection method show the *Sm*ADSL activity in presence of Adenosylsuccinate (ADS) resulting in an endothermic reaction ($\Delta H_{app} = 9.0 \pm 0.2$ kcal/mol). (B) Analogously, the ΔH_{app} obtained from single injection using SAICAR resulting in an endothermic reaction above (4.7 ± 1.3) kcal/mol. (C) The Michaelis-Menten fit using a single binding model from the multiple injection method show the enzymatic activity in ADS consumption with a K_M of 17.2 ± 2.3 μ M and $k_{cat} = 0.73 \pm 0.04$ s^{-1} . *Inset*: raw data. (D) The kinetics assays using multiple injection method show the enzymatic activity to SAICAR consumption presenting a $K_M = (5.3 \pm 1.2)$ μ M and $k_{cat} = 1.8 \pm 0.3$ s^{-1} . *Inset*: raw data.

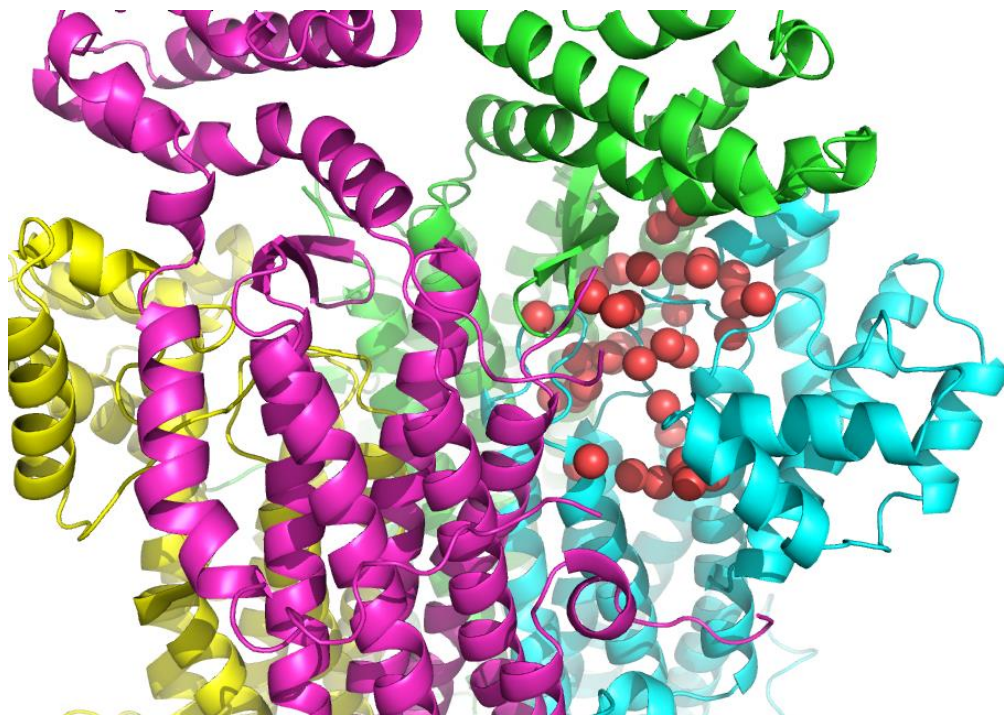


Figure 2. Cartoon diagrams of the *SmADSL*: zoom-in view of the active site. Forty water molecules (red spheres) are present in the active site related with the high entropy important to kinetic reaction.

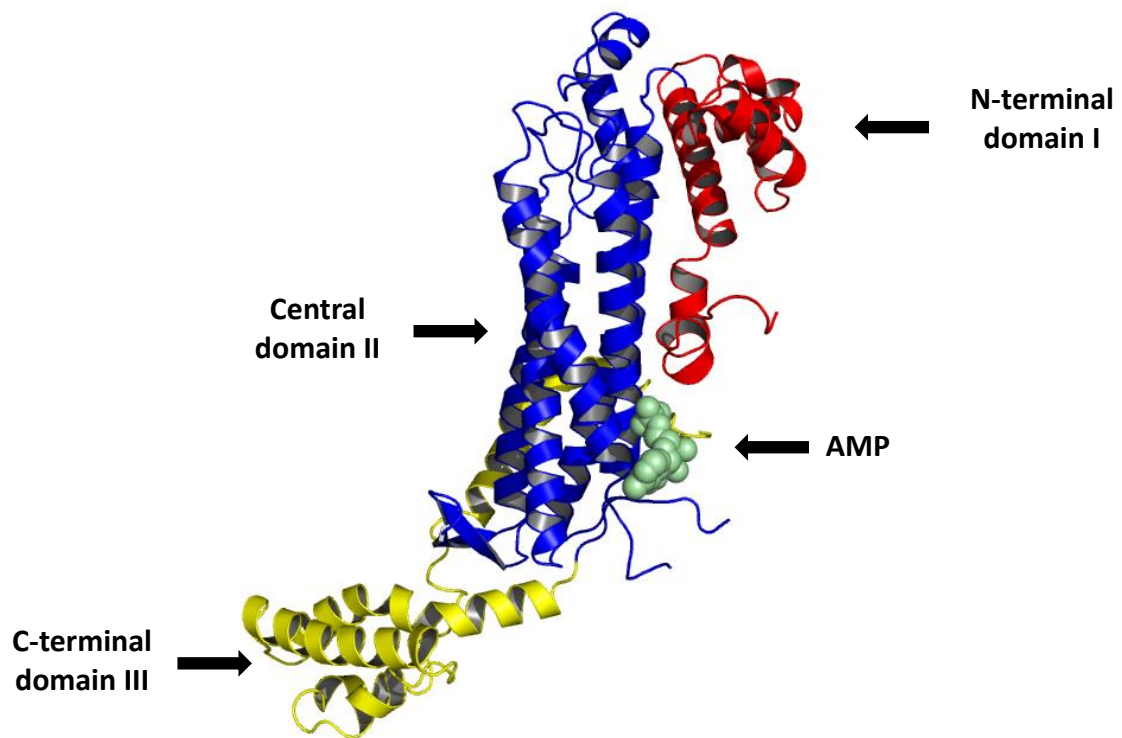
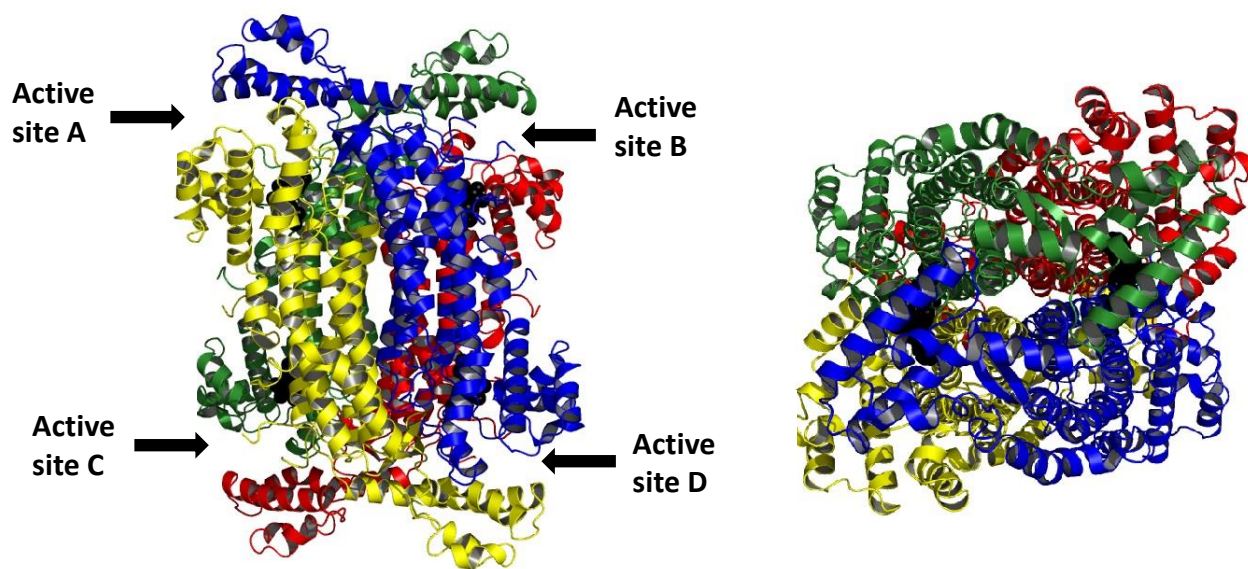


Figure 3. *SmADSL* monomer can be divided into three domains that combine to form an elongated structure. Domain I (red) comprises residues 1 – 101, which form six helices ($\alpha 1 - \alpha 7$). Domain II (blue), consisting of residues 102 – 358, forms an elongated helical bundle assembled by $\alpha 8$ through $\alpha 15$ as well as a short two-stranded antiparallel β -strands ($\beta 1, \beta 2$) positioned between $\alpha 8$ and $\alpha 9$. Domain III (yellow) comprises nine helices ($\alpha 16 - \alpha 25$) constructed from residues 359 – 480.



689

690 Figure 4. Cartoon diagrams of the *SmADSL* tetramer, the active enzyme. Subunit A is
 691 coloured green, B is red, C is yellow and subunit D is coloured blue. AMP is black.

692

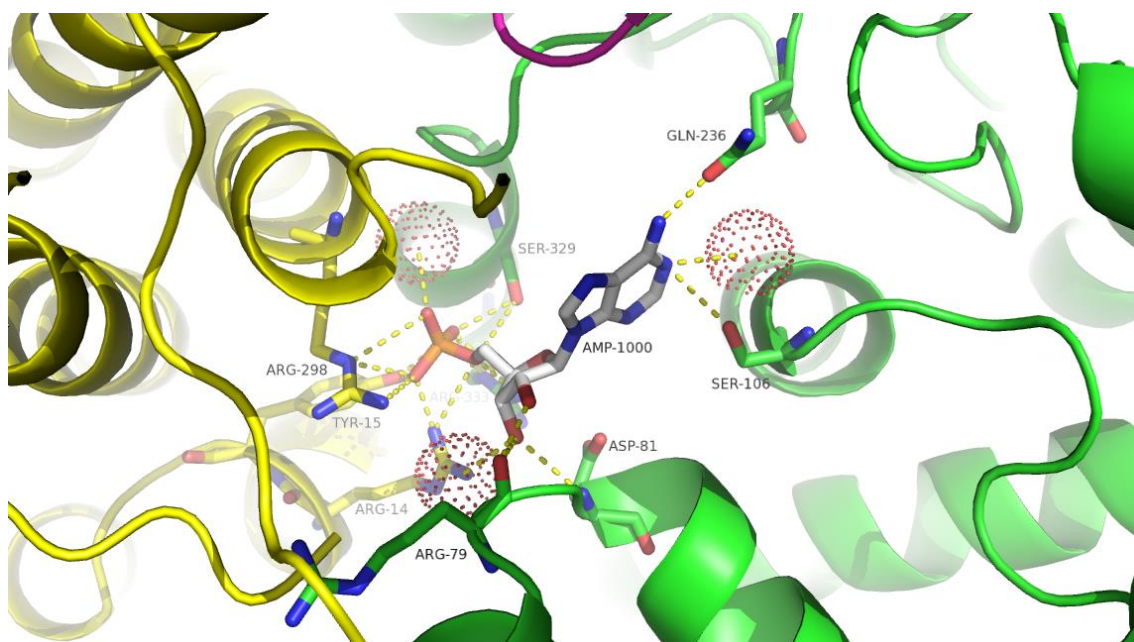


Figure 5. AMP-binding site of the *SmADSL*–AMP ternary complex. Monomer A – green and Monomer C – yellow. AMP phosphate accepts hydrogen bonds from Arg14C, Tyr15C, Arg298C, Ser329A, Arg333A and water. The ribose O2 donates a hydrogen bond to the Arg79A carbonyl and O3 accepts hydrogen bonds from the carbonyl of Arg79A, Asp81A NH2 and water. The adenine N1 accepts a hydrogen bond from Ser106A and water; N6 donates hydrogen bonds to Gln236A

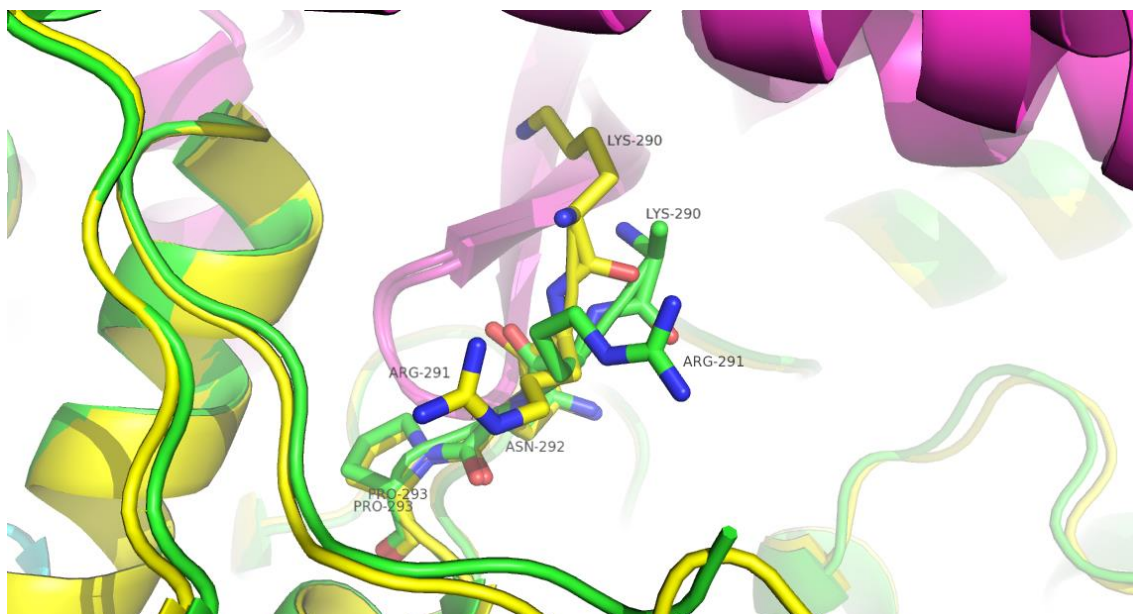


Figure 6. Superposed of the disordered loop signature sequence $^{281}\text{Q}^*\text{GSS}^*\text{MP}^*\text{K}^*\text{NP}^{293}$ unique to the superfamily β -elimination in the *SmADSL*-AMP (yellow) and the *SmADSL*-Apo (green). In the *SmADSL*-AMP structure, the side chain of Arg291 is down and away from the active site while the *SmADSL*-Apo structure the side chain of Arg291 is into the active site. In *SmADSL*-AMP, Lys290 moves away from the active site than in *ADSL*-Apo structure.